Solvent Annealed Thin Films of Asymmetric Polyisoprene−Polylactide Diblock Copolymers

Kevin A. Cavicchi[†] and Thomas P. Russell*

Department of Polymer Science and Engineering, University of Massachusetts, Amherst, Massachusetts 01003

Received May 23, 2006; Revised Manuscript Received December 18, 2006

ABSTRACT: A poly(isoprene-*b*-lactide) (PI-*b*-PLA) polymer forming cylinders of PLA in a PI matrix was examined as a polymer system to generate nanostructured vertical arrays of hexagonally packed cylinders. This investigation was motivated by the favorable properties of PI-*b*-PLA for fabricating nanoporous materials. Films were swollen and annealed with chloroform over a range of thickness and solvent concentration. Examination of the films after swelling with scanning force microscopy and grazing incidence X-ray scattering showed that films with either parallel or perpendicular domain orientations could be obtained. The domain orientation depends on the selectivity of the film surface, mediated by the concentration of chloroform, and the incommensurability of the polymer domain spacing and the swollen film thickness. The results show that solvent annealing is an effective method for obtaining oriented PI-*b*-PLA cylinder templates and more generally an effective method for obtaining perpendicularly oriented cylinders over a wide area from an initially unoriented film.

Introduction

The self-assembled morphologies of block copolymers represent an ideal platform for the fabrication of nanostructured thin films.[1] Thin films of cylinder-forming block copolymers, with the cylinders oriented normal to the surface, are attractive as templates for the formation of ordered arrays of domains with high aspect ratios. One goal in nanopatterning is to shrink the domain size and obtain higher domain densities. In block copolymers the domain size is controlled primarily by the molecular weight of the polymer. For each copolymer system there is a minimum domain size obtainable due to the order−disorder transition temperature that occurs at a critical value of χN, where χ is the Flory−Huggins interaction parameter and N is the degree of polymerization of the polymer.[2] Therefore, using high-χ materials lowers the chain length at which the copolymers microphase separate, producing materials with smaller domain sizes and higher domain densities.

We have investigated thin films of poly(isoprene-*b*-lactide) (PI-*b*-PLA) block copolymers.[3] The motivation for studying this particular system was twofold. First, with a polymer that forms cylinders of PLA in a matrix of PI, it should be possible to cross-link the PI and hydrolytically degrade the PLA to produce a nanoporous film.[4] Second, compared to other polymer systems that have previously been used to make nanoporous thin films, such as poly(styrene-*b*-methyl methacrylate) (PS-*b*-PMMA),[5] poly(styrene-*b*-isoprene) (PS-*b*-PI),[6] and poly(styrene-*b*-lactide) (PS-*b*-PLA),[7] PI-*b*-PLA has a larger χ and therefore smaller pores, and a higher pore density should be obtainable with this polymer. For example, at 140 °C the χ is 0.04 for PS-*b*-PMMA,[8] 0.06 for PS−PI,[9] 0.13 for PS-*b*-PLA,[4] and 0.3 for PI-*b*-PLA.[10,11]

The main challenge in using block copolymers as nanostructured templates is that in anisotropic morphologies, like cylinders, the preferential interaction of one block with the substrate leads to an alignment of the microdomains parallel to the surface. Recent simulations on the morphologies in thin films of cylinder-forming block copolymers confined between two surfaces showed that the morphology depended on the strength of the interfacial interactions and commensurability between the copolymer period and film thickness,[12,13] similar to results previously shown for lamellar forming copolymers.[14−18] The preferential segregation of one block to the substrate causes an orientation of the microdomains parallel to the substrate. With increasing surface selectivity, morphologies from parallel cylinders to perforated lamellae to lamellae are found. Incommensurability between the natural period of the copolymer and the film thickness gives rise to chain stretching that can induce an orientation of the microdomains normal to the surface, even in the presence of preferential interfacial interactions. With balanced interfacial interactions, the microdomains orient normal to the surface, and consequently, commensurability is not an issue. Complementary experiments were run on polystyrene−polybutadiene−polystyrene (PS-*b*-PB-*b*-PS) triblock copolymers by swelling them to different extents in chloroform, to vary both the surface selectivity and film thickness, and then quickly evaporating the solvent to preserve the surface structure.[12,19] These annealed films had terraced surfaces with varying local thickness. Subsequent scanning force microscopy (SFM) measurements over thickness gradients in the films revealed variations in the surface structure similar to those predicted by the simulations.

We recently reported that in a cylinder-forming PI-*b*-PLA thin film that a perpendicular orientation over a large area with long-range order could be obtained by swelling the film with chloroform.[3] In this report we describe further solvent annealing experiments to study the roles of both solvent concentration and film thickness incommensurability on the domain orientation of a PI-*b*-PLA block copolymer. Both scanning force microscopy and GISAXS measurements were used to characterize both the film surface and subsurface structure. The results are consistent with prior solvent annealing experiments on SBS.[12,19] However, it is notable in this case that films with a perpendicular orientation over the entire film could be obtained rather than just between steps of parallel cylinders. These experiments are also different from cases where perpendicular cylinders are obtained during solvent casting.[20,21] Here the orientation is

[†] Current address: Department of Polymer Engineering, University of Akron, Akron, OH 44325.

10.1021/ma061163w CCC: $37.00
Published on Web 01/24/2007

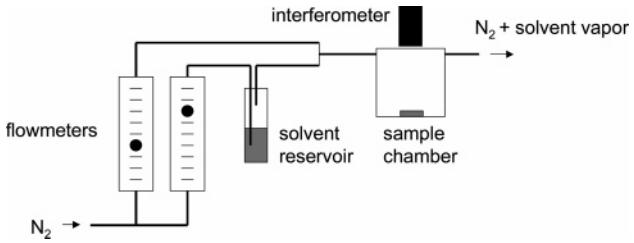

Figure 1. Schematic of experimental setup used for solvent annealing.

driven by an advancing solvent evaporation front during ordering. As this polymer system has desirable traits for fabricating high-density nanoporous templates, understanding how to control the thin film morphology is the first step toward obtaining useful templates.

Experimental Section

Materials. The polymer used in this work was a poly(isoprene-*b*-lactide) (PI-*b*-PLA) block copolymer (M_n = 22 000 Da, f_{PI} = 0.78). It was prepared using a previously reported method.[10] The molecular weight of the PI block was determined using size exclusion chromatography (SEC), calibrated with PS standards. The molecular weight and volume fraction of the PLA block were determined using ^{1}H NMR spectroscopy (300 MHz). The solvents for annealing, cross-linking, and PLA degradation were used as received.

Sample Preparation and Solvent Annealing. Thin films of PI-*b*-PLA were prepared by spin-coating solutions of PI-*b*-PLA in chloroform (8−11 mg/mL) at 2000 rpm onto silicon wafers with a native oxide surface layer (1 × 1 cm). Thicker silicon wafers were used to provide flat substrates for the grazing incidence X-ray scattering measurements.

Solvent annealing was done using an apparatus that is schematically shown in Figure 1. The concentration of solvent in the chamber was controlled by varying the flow rates (5−49 mL/min) of the pure and solvent infused nitrogen. An interferometer (Filmetrics F20) was used to measure the thickness of the film during annealing. Solvent was removed from the film by turning up the pure nitrogen flow rate to its maximum rate and stopping the flow of solvent infused nitrogen. The thickness of the unswollen sample is t_0. The thickness of the swollen sample is t_s. The volume fractions of polymer, ϕ_p, and solvent, ϕ_s, in the swollen sample are given by $\phi_p = t_0/t_s$ and $\phi_s = 1 - \phi_p$. Scanning force microscopy (SFM) measurements were made using a Dimension 3100 Nanoscope III SFM (Digital Instruments) in tapping mode. Both the effect of solvent concentration and film thickness on the film morphology were examined by first varying the degree of swelling on a set of samples of the same film thickness and then repeating these experiments on sample sets over a range of unswollen thickness of 48−71 nm. Each sample was annealed for 30−60 min.

Cross-linking of PI was done using sulfur monochloride vapor.[22] Films were taped to a glass slide and placed in a closed container containing a small amount of sulfur monochloride liquid. After 1 h the films were removed and washed in toluene. The PLA was degraded by immersing cross-linked films in solutions of 1 M tetrabutylammonium fluoride in tetrahydrofuran.

Modified substrates were prepared by spin-coating the PI-OH precursor to this block copolymer on silicon substrates and annealing the substrates at 150 °C under vacuum for 24 h. Condensation of the hydroxyl group with surface silanol groups on the native oxide layer of silicon substrate forms a PI brush.[23] Excess polymer was removed by washing the substrates repeatedly with toluene.

Small-Angle X-ray Scattering (SAXS). Measurements were made using a Molecular Metrology instrument. The sample-to-detector distance was calibrated using a silver behenate standard.

Grazing Incidence Small-Angle X-ray Scattering (GISAXS). Measurements were performed at beamline I15-D at the Advanced Photon Source, Argonne National Lab. Samples were mounted on a goniometer, and measurements were taken at incident angles between 0.1° and 0.3°. The sample-to-detector distance was calibrated using a silver behenate standard. A schematic of the experiment is shown in Figure 2.

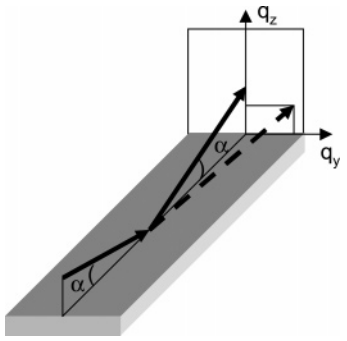

Figure 2. Schematic representation of the GISAXS experiment. The beam is incident on the sample at an angle α. There is a specular reflection at an angle α. The dotted line indicates an off-specular scattering in the q_y-q_z plane.

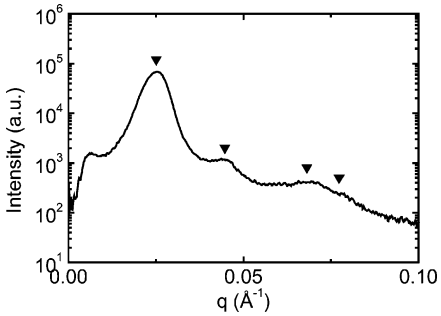

Figure 3. Azimuthally averaged SAXS profile of bulk PI-*b*-PLA polymer at 100 °C. The triangles indicate q/q^* peak positions of 1, $\sqrt{3}$, $\sqrt{7}$, and $\sqrt{9}$.

Results and Discussion

The bulk morphology of the PI-*b*-PLA polymer was determined using small-angle X-ray scattering. Figure 3 shows an azimuthally averaged intensity profile for a sample annealed at 100 °C. The peaks at q/q^* ratios of 1, $\sqrt{3}$, $\sqrt{7}$, and $\sqrt{9}$ are consistent with the structure factor for hexagonally packed cylinders. (The expected peak at $q/q^* = \sqrt{4}$ is absent due to form factor cancellation.[24])

Thin Films Morphology. The morphology of the as-spun film was examined with SFM. Figure 4a shows a phase image of a typical as-spun film. The morphology consists of bright lines and dots on a dark background. These bright regions are attributed to the PLA, which as the higher modulus material would appear brighter in the phase image and is consistent with the bulk morphology of the polymer. After solvent annealing three types of surface patterns were observed with SFM consisting of lines (4b), a mixture of lines and dots (4c), or dots (4d). These are consistent with cylindrical microdomains oriented parallel to the surface (4b), a mixture of parallel and perpendicular orientations of the cylindrical microdomains (4c), and cylindrical microdomains oriented perpendicular to the surface (4d). Figure 5 shows optical micrographs of films with different domain orientations. When the cylindrical microdomains are oriented parallel to the surface (Figure 5a), the surface of the film is terraced to relieve frustration arising from the film thickness constraints. Terracing has been observed previously in block copolymer thin films where either islands or holes develop to form areas whose film thickness is commensurate with the domain spacing.[25] With a perpendicular

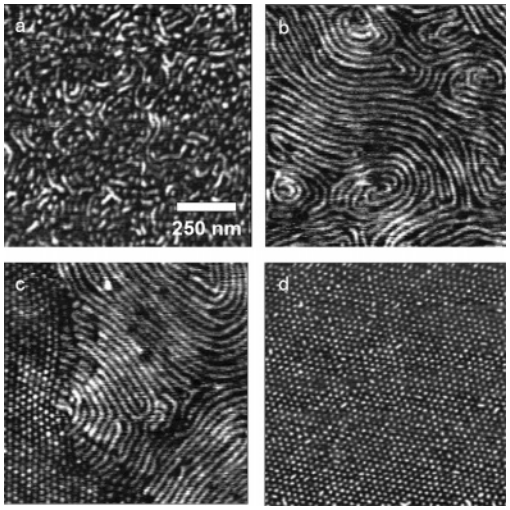

Figure 4. SFM phase images of PI-*b*-PLA thin films (a) as spun (t_0 = 49 nm) and after solvent annealing, (b) parallel orientation (t_0 = 65 nm, 33% $CHCl_3$), (c) mixed parallel and perpendicular orientations (t_0 = 65 nm, 38% $CHCl_3$), and (d) perpendicular orientation (t_0 = 45 nm, 38% $CHCl_3$).

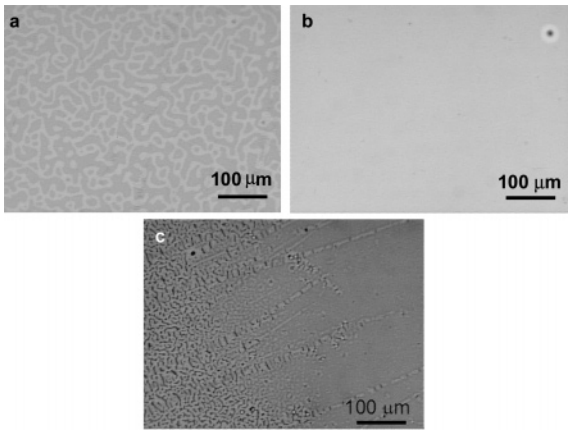

Figure 5. Optical micrographs of annealed films with a (a) parallel orientation (t_0 = 71 nm, 44% $CHCl_3$), (b) perpendicular orientation (t_0 = 49 nm, 41% $CHCl_3$), and (c) both parallel and perpendicular orientations near the film edge (t_0 = 49 nm, 38% $CHCl_3$).

orientation (Figure 5b), there are gradual changes in the film thickness since there are no thickness constraints. Figure 5c was taken near the edge of a film where the thickness increases near the film edge in a spin-coated film. Half of the surface is smooth (perpendicular orientation) while the other half is rough due to the terracing of film (parallel orientation). The degree of long-range order is much higher in the perpendicular films compared to the parallel. Indeed, six-spot patterns were sometimes observed in the Fourier transform of 2 × 2 μm SFM images, indicating the presence of a single grain; however, 12- and 18-spot patterns or spot and arc patterns were more commonly observed, indicating the presence of more granular texture, and the typical grain size was on the order of 0.5−1 μm. The much poorer ordering in the parallel structures is likely due to the terracing impeding ordering, but in both cases the long-range order is substantially improved compared to the as-spun film.

GISAXS measurements were used to complement the SFM measurements. SFM gives a real-space surface image of a small area of the film, while GISAXS averages over a much larger area and can be used to probe the structure through the entire thickness of the film.[3,26−31] Analytical descriptions of GISAXS patterns have been given using the distorted wave Born approximation.[31−33] GISAXS patterns are generally more complicated to interpret than transmission SAXS, since scattering can occur with both the incident and reflected beams. The GISAXS patterns can be viewed as two overlaying scattering patterns from the direct and reflected beam.[31] Figure 6 shows a schematic diagram of the real-space and reciprocal space lattices of cylindrical microdomains oriented parallel and perpendicular to the film surface. With the beam incident along the q_x direction, cylinders oriented parallel to the film surface give rise to a six-spot pattern, while when the cylindrical microdomains are oriented normal to the surface, a series of spots along the q_y axis are seen.

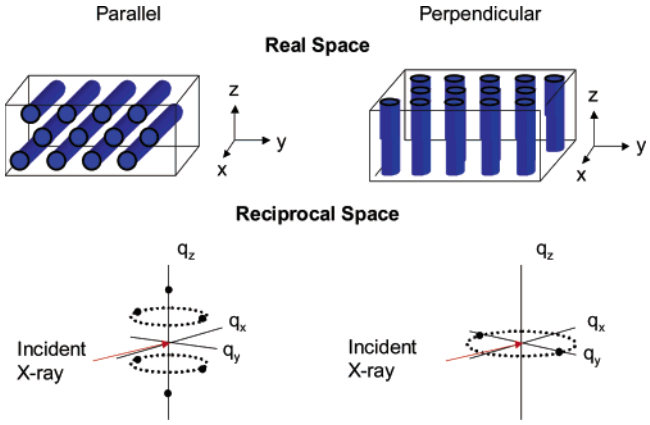

Figure 6. Schematic diagram of real-space and reciprocal-space lattices of parallel and perpendicular cylinders.

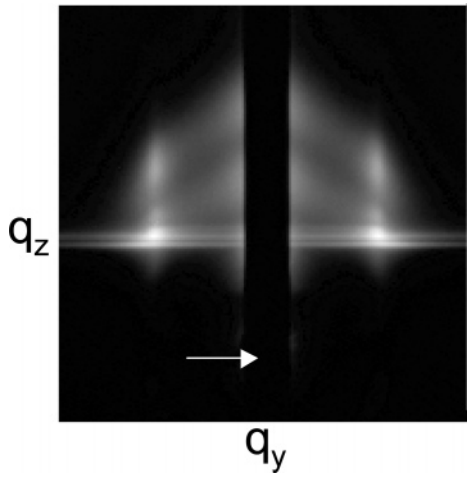

Figure 7. (a) GISAXS pattern from a PI-*b*-PLA film with a parallel orientation (t_0 = 71 nm, 44% $CHCl_3$) at α = 0.2°. The arrow indicates the position of the direct beam at q_y = 0 and q_z = 0.

Figure 7 shows a GISAXS pattern from a film with the cylindrical microdomains oriented parallel to the film surface (t_0 = 71 nm, 44% $CHCl_3$) taken at α = 0.2°. Two arcs can be seen around the specular reflection. Each arc has three spots: one on either side of the beam stop and one partially obscured by the beam stop. These spots arise from the cylindrical microdomains oriented with the (10) planes parallel to the substrate, as shown in Figure 6. The bottom halves of the diffraction rings are obscured by the sample horizon. The arcs at lower and higher q_z arise from the scattering from the direct and reflected beams, respectively.

Figure 8a shows a GISAXS pattern for a sample with the cylindrical microdomains oriented normal to the surface at α = 0.2° (t_0 = 49 nm, 41% $CHCl_3$). A streak, rather than a spot, is observed on either side of the specular reflection. The streak arises from the truncation of the cylindrical microdomains at the surface in the thin film, giving rise to Bragg rods in

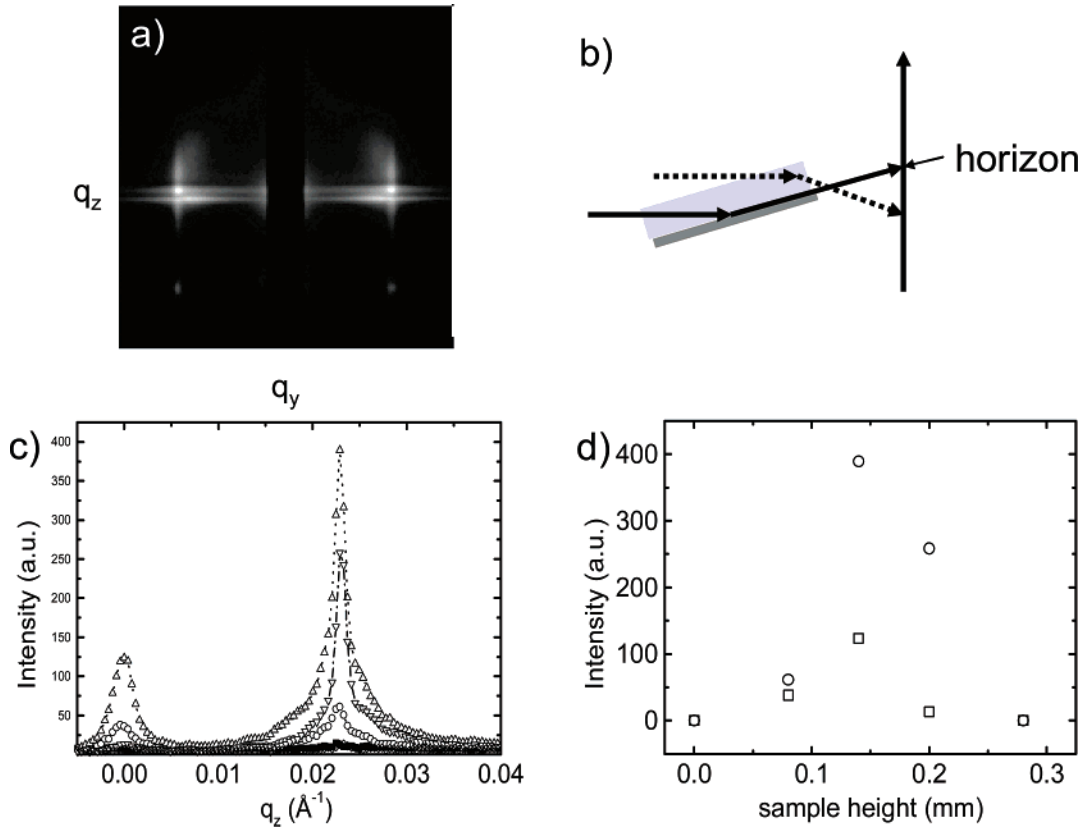

Figure 8. (a) GISAXS pattern of PI-*b*-PLA with a perpendicular orientation ($t_0 = 49$ nm, 41% $CHCl_3$) at $\alpha = 0.2$. (b) Schematic diagram of how scattering below the horizon arises from the sample edge. (c) Intensity vs q_z at $q_y = 0.03$ Å^{-1} as a function of the sample position y: (■) $y = 0$, (○) $y = 0.08$ mm, (△), $y = 0.14$ mm, (▽) $y = 0.2$ mm, (◇) $y = 0.28$ mm at $\alpha = 0.16$. (d) Peak intensity at $q_y = 0.03$ Å^{-1} vs sample height; (□) $q_z = 0$ Å^{-1}, (○) $q_z = 0.023$ Å.[1]

reciprocal space.[34] Also, there is a spot on either side of the direct beam. As shown schematically in Figure 8b, if the sample is positioned in the beam such that the incident beam can pass through the edge of the sample, as shown by the dotted arrows, then the scattering will not be attenuated by the substrate. Figure 8c shows plots of intensity vs q_z at $q_y = 0.03$ at different sample heights y, and Figure 8d is a plot of the peak intensity. At $y = 0$, the sample is below the beam and the scattered intensity is zero. As the sample is raised into the beam, some of the beam is able to pass through the sample edge, and scattering is detected below the sample horizon. However, once the sample is raised high enough ($y = 0.2$ mm), the beam is no longer able to pass through the film without passing through the substrate, and no scattering is observed below the sample horizon. Therefore, examining the scattering around the direct beam can give information about the sample edge. Figure 9 shows a GISAXS pattern of a different sample with cylindrical microdomains oriented normal to the surface ($t_0 = 53$ nm, 44% $CHCl_3$). The Bragg rods are clearly evident, but there are weaker spots observed at smaller values of q_y which arise from regions where the cylindrical microdomains are oriented parallel to the surface near the sample edge, as observed in Figure 5c. Two sets of four spots can be seen arising from the scattering from the incident and reflected beams. By considering the GISAXS, SFM, and optical microscopy measurements as a whole, an unambiguous determination of the film morphology can be made, which would be more difficult by one of these techniques alone.

Orientation Control. As commensurability and surface energy have been shown to be driving forces in orienting the microdomains in thin films, an orientation diagram was constructed by plotting the observed domain orientation as a function of the swollen film thickness vs the volume fraction of chloroform in the swollen film (Figure 10). These diagrams show that the orientation change is not solely driven by commensurability; otherwise, an orientation of the microdomains normal to the surface would be expected regardless of the concentration of chloroform in the swollen film. A perpendicular orientation of the microdomains occurs at higher concentrations of chloroform in the swollen film. Therefore, the solvent must mediate the interfacial interactions to make the interfaces less selective to either block. The boundary between the parallel and perpendicular orientation of the microdomains has a sawtooth-type pattern. This is consistent with the perpendicular orientation of the microdomains becoming more energetically favorable

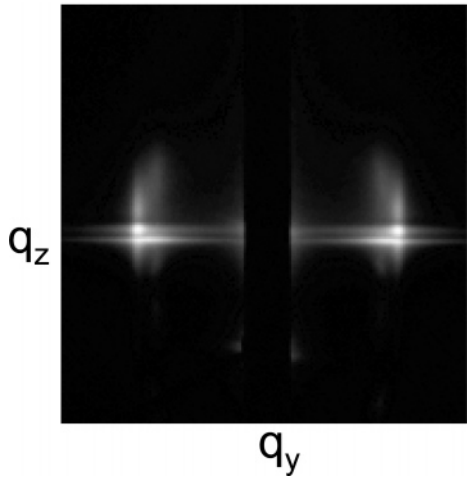

Figure 9. GISAXS pattern of a sample with perpendicular cylinders at $\alpha = 0.2°$ ($t_0 = 53$ nm, 44% $CHCl_3$).

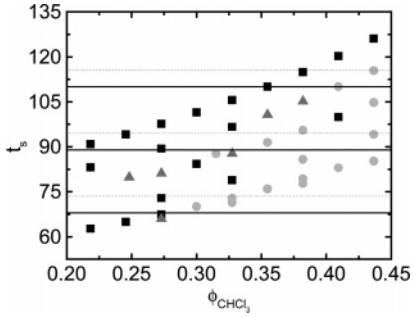

Figure 10. Orientation diagram of PI-*b*-PLA thin films as a function of the swollen film thickness (t_s) and the concentration in the swollen film: (black ■) parallel, (gray ●) perpendicular, (gray ▲) mixed parallel and perpendicular. The dotted lines are drawn at $t_s = d_{10}(n + 0.5)$ for $n = 3$, 4, and 5. The solid lines are drawn at $t_s = d_{10}(n + 0.5) + w$ for $n = 2$, 3, and 4 with $w = 15.5$ nm.

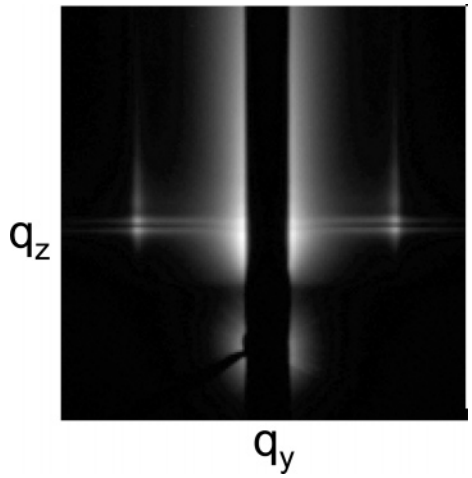

Figure 11. GISAXS pattern of a cross-linked PI-*b*-PLA thin film with a perpendicular cylinder orientation ($t_0 = 49$ nm, 38% $CHCl_3$).

than the parallel orientation when the film thickness is incommensurate with the domain spacing of the cylindrical microdomains. Consequently, the orientation of the microdomains normal to the film surface should extend to lower solvent concentrations (higher surface selectivity) when incommensurability between the domain spacing and film thickness is maximized, i.e., when $t_s = d_{10}(n + 0.5)$. The domain spacing, d_{10}, was determined to be 21 nm in the GISAXS patterns of the films with the cylindrical microdomains oriented normal to the surface. Using this domain spacing, the dotted lines in Figure 10 were drawn for $n = 3$, 4, and 5. These lines overestimate the position where incommensurability is maximal due, more than likely, to a wetting layer of PI-*b*-PLA at the substrate, since the native oxide of the substrate preferentially interacts with the PLA block. Therefore, maximal incommensurability with the film thickness occurs when $t_s = d_{10}(n + 0.5) + w$, where w is the wetting layer thickness. The solid lines in Figure 11 were calculated for $n = 2$, 3, and 4 with a wetting layer thickness of 15.5 nm. This is slightly thicker than $d_{10}/2$, which would be the simplest approximation of the wetting layer thickness, assuming a single layer of chains at the substrate interface. However, this is consistent with results for PS-*b*-PB-*b*-PS triblock thin films where a wetting layer larger than $d_{10}/2$ was also observed.[19] Previous measurements indicated that an ordering transition occurred at ~40% $CHCl_3$ for this polymer.[3] Here, commensurability effects are observed up to 44% $CHCl_3$, indicating that the films are still ordered at this concentration. There is some uncertainty in both film thickness measurements. However, if the swollen thickness of the films is less, the points would shift down and to the left, indicating a smaller wetting layer thickness. The presence of a wetting layer with a perpendicular orientation is very interesting. It indicates that the solvent mediates the interactions at the air surface, making a perpendicular orientation favorable at high film thickness incommensurability. However, at the same time the solvent cannot fully mediate the interactions at the substrate, and a wetting layer is still obtained due to a preference for one of the blocks. Wetting layers have previously been observed in perpendicularly oriented PS-*b*-PLA thin films on native oxide surfaces and in PS-*b*-PB-*b*-PS thin films annealed with chloroform vapor.[19,35] In simulations of thin films of cylinder-forming copolymers with dissimilar interfaces perpendicular orientations with a substrate wetting layer have been observed.[36]

Cross-Linking and Degradation. While the wetting layer is of fundamental importance, it causes difficulties in the subsequent processing of these films. To prepare nanoporous films by selectively etching the PLA domains, the PI domains must first be cross-linked. After cross-linking the PI domains with sulfur monochloride vapor the films were insoluble in organic solvent. Attempts to characterize cross-linked films by SFM measurements were unsuccessful with no contrast observed in either the height or phase SFM images. Figure 11 shows a GISAXS pattern of a cross-linked film with the cylindrical microdomains oriented normal to the film surface ($t_0 = 49$ nm, 38% $CHCl_3$). This pattern is similar to the pattern in Figure 8a. This demonstrates that the cross-linking does not adversely affect the morphology of the thin film. When cross-linked films were immersed in a 1 M solution of tetrabutylammonium fluoride (TBAF) in tetrahydrofuran to degrade the PLA,[37] they no longer adhered to the substrate due to the etching of the PLA wetting layer, and parts of the film could be seen floating in the solution. To produce films without a wetting layer, silicon substrates with a homopolymer PI brush were used. After spin-coating and cross-linking the films treated with a TBAF solution remained intact on the substrate. The as-spun films had a similar surface morphology as on the unmodified substrates. Preliminary solvent annealing of these films resulted in mixed orientations. These results are encouraging, and further investigations will examine controlling the domain orientation with solvent annealing on modified substrates.

Conclusions

The morphology of solvent annealed PI-*b*-PLA thin films was investigated. It was found that by controlling both the swollen film thickness and the concentration of solvent in the swollen film whole films with either parallel or perpendicular cylinder orientations could be obtained. Investigation of the orientation behavior with film thickness indicated that a wetting layer of PLA existed in all orientations after solvent annealing, which was further confirmed by cross-linking and degradation experiments. The ability to control the orientation in PI-*b*-PLA films is the first step in developing a new system for block copolymer templating.

Acknowledgment. We acknowledge funding for this work from Seagate Technology LLC, the NSF supported Materials Research Science and Engineering Center at UMASS, and the Department of Energy under DE-FG-96ER45612. Use of the Advanced Photon Source was supported by the U.S. Department of Energy, Office of Science, Office of Basic Energy Sciences, under Contract DE-ACO2-06CH11357. We thank David Cookson (APS) for his assistance and for helpful discussions during our GISAXS measurements.

References and Notes

(1) Park, C.; Yoon, J.; Thomas, E. L. *Polymer* **2003**, *44*, 6725−6760.
(2) Matsen, M. W.; Bates, F. S. *Macromolecules* **1996**, *29*, 1091−1098.
(3) Cavicchi, K. A.; Berthiaume, K. J.; Russell, T. P. *Polymer* **2005**, *46*, 11635−11639.
(4) Zalusky, A. S.; Olayo-Valles, R.; Wolf, J. H.; Hillmyer, M. A. *J. Am. Chem. Soc.* **2002**, *124*, 12761−12773.
(5) Thurn-Albrecht, T.; Steiner, R.; DeRouchey, J.; Stafford, C. M.; Huang, E.; Bal, M.; Tuominen, M.; Hawker, C. J.; Russell, T. P. *Adv. Mater.* **2000**, *12*, 787−790.
(6) Park, M.; Harrison, C.; Chaikin, P. M.; Register, R. A.; Adamson, D. H. *Science* **1997**, *276*, 1401−1404.
(7) Leiston-Belanger, J. M.; Russell, T. P.; Drockenmuller, E.; Hawker, C. J. *Macromolecules* **2005**, *38*, 7676−7683.
(8) Russell, T. P.; Hjelm, R. P., Jr.; Seeger, P. A. *Macromolecules* **1990**, *23*, 890−893.
(9) Lodge, T. P.; Pan, C.; Jin, X.; Liu, Z.; Zhao, J.; Maurer, W. W.; Bates, F. S. *J. Polym. Sci., Part B: Polym. Phys.* **1995**, *33*, 2289−2293.
(10) Schmidt, S. C.; Hillmyer, M. A. *Macromolecules* **1999**, *32*, 4794−4801.
(11) Schmidt, S. C.; Hillmyer, M. A. *J. Polym. Sci., Part B: Polym. Phys.* **2002**, *40*, 2364−2376.
(12) Knoll, A.; Horvat, A.; Lyakhova, K. S.; Krausch, G.; Sevink, G. J. A.; Zvelindovsky, A. V.; Magerle, R. *Phys. Rev. Lett.* **2002**, *89*, 035501−03550.4.
(13) Horvat, A.; Lyakhova, K. S.; Sevink, G. J. A.; Zvelindovsky, A. V.; Magerle, R. *J. Chem. Phys.* **2004**, *120*, 1117−1126.
(14) Kellogg, G. J.; Walton, D. G.; Mayes, A. M.; Lambooy, P.; Russell, T. P.; Gallagher, P. D.; Satija, S. K. *Phys. Rev. Lett.* **1996**, *76*, 2503−2506.
(15) Lambooy, P.; Russell, T. P.; Kellogg, G. J.; Mayes, A. M.; Gallagher, P. D.; Satija, S. K. *Phys. Rev. Lett.* **1994**, *72*, 2899−2902.
(16) Walton, D. G.; Kellogg, G. J.; Mayes, A. M.; Lambooy, P.; Russell, T. P. *Macromolecules* **1994**, *27*, 6225−6228.
(17) Fasolka, M. J.; Banerjee, P.; Mayes, A. M.; Pickett, G.; Balazs, A. C. *Macromolecules* **2000**, *33*, 5702−5712.
(18) Turner, M. S. *Phys. Rev. Lett.* **1992**, *69*, 1788−1791.
(19) Knoll, A.; Magerle, R.; Krausch, G. *J. Chem. Phys.* **2004**, *120*, 1105−1116.
(20) Lin, Z.; Kim, D. H.; Wu, X.; Boosahda, L.; Stone, D.; LaRose, L.; Russell, T. P. *Adv. Mater.* **2002**, *14*, 1373−1376.
(21) Harant, A. W. *J. Vac. Sci. Technol. B* **2005**, *23*, 1615−1621.
(22) Glazer, J. *J. Polym. Sci.* **1954**, *14*, 225−240.
(23) Mansky, P.; Liu, Y.; Huang, E.; Russell, T. P.; Hawker, C. *Science* **1997**, *275*, 1458−1460.
(24) Forster, S.; Timmann, A.; Konrad, M.; Schellbach, C.; Meyer, A.; Funari, S. S.; Mulvaney, P.; Knott, R. *J. Phys. Chem. B* **2005**, *109*, 1347−1360.
(25) Coulon, G.; Russell, T. P.; Deline, V. R.; Green, P. F. *Macromolecules* **1989**, *22*, 2581.
(26) Xu, T.; Goldbach, J. T.; Misner, M. J.; Kim, S.; Gibaud, A.; Gang, O.; Ocko, B.; Guarini, K. W.; Black, C. T.; Hawker, C. J.; Russell, T. P. *Macromolecules* **2004**, *37*, 2972−2977.
(27) Tang, C.; Tracz, A.; Kruk, M.; Zhang, R.; Smilgies, D.-M.; Matyjaszewski, K.; Kowalewski, T. *J. Am. Chem. Soc.* **2005**, *127*, 6918−6919.
(28) Papadakis, C. M.; Busch, P.; Posselt, D.; Smilgies, D.-M. *Adv. Solid State Phys.* **2004**, *44*, 327−338.
(29) Li, M.; Douki, K.; Goto, K.; Li, X.; Coenjarts, C.; Smilgies, D. M.; Ober, C. K. *Chem. Mater.* **2004**, *16*, 3800−3808.
(30) Du, P.; Li, M.; Douki, K.; Li, X.; Garcia, C. B. W.; Jain, A.; Smilgies, D.-M.; Fetters, L. J.; Gruner, S. M.; Wiesner, U.; Ober, C. K. *Adv. Mater.* **2004**, *16*, 953−957.
(31) Lee, B.; Park, I.; Yoon, J.; Park, S.; Kim, J.; Kim, K.-W.; Chang, T.; Ree, M. *Macromolecules* **2005**, *38*, 4311−4323.
(32) Rauscher, M.; Salditt, T.; Spohn, H. *Phys. Rev. B: Condens. Matter* **1995**, *52*, 16855−16863.
(33) Vineyard, G. H. *Phys. Rev. B: Conden. Matter Mater. Phys.* **1982**, *26*, 4146−4159.
(34) Smilgies, D. M.; Busch, P.; Papadakis, C. M.; Posselt, D. *Synchrotron Radiat. News* **2002**, *15*, 35−41.
(35) Olayo-Valles, R.; Lund, M. S.; Leighton, C.; Hillmyer, M. A. *J. Mater. Chem.* **2004**, *14*, 2729−2731.
(36) Lyakhova, K. S.; Sevink, G. J. A.; Zvelindovsky, A. V.; Horvat, A.; Magerle, R. *J. Chem. Phys.* **2004**, *120*, 1127−1137.
(37) Nouvel, C.; Dubois, P.; Dellacherie, E.; Six, J.-L. *J. Polym. Sci., Part A: Polym. Chem.* **2004**, *42*, 2577−2588.

MA061163W